Available online at www.sciencedirect.com

ScienceDirect

Journal of Electrical Systems and Information Technology 4 (2017) 347–358

www.elsevier.com/locate/jesit

Design of PR current control with selective harmonic compensators using Matlab

Daniel Zammit *, Cyril Spiteri Staines, Maurice Apap, John Licari

Department of Industrial Electrical Power Conversion, University of Malta, Msida, MSD 2080, Malta

Received 10 November 2015; received in revised form 7 November 2016; accepted 10 January 2017
Available online 25 January 2017

Abstract

This paper presents a procedure to design a Proportional Resonant (PR) current controller with additional PR selective harmonic compensators for Grid Connected Photovoltaic (PV) Inverters. The design of the PR current control and the harmonic compensators will be carried out using Matlab. Testing was carried out on a 3 kW Grid-Connected PV Inverter which was designed and constructed for this research. Both simulation and experimental results will be presented.

Keywords: Inverters; Proportional-resonant controllers; Harmonic compensation; Photovoltaic; Matlab; SISO design tool

1. Introduction

Harmonics generated by Distributed Power Generation Systems is a major power quality issue, especially due to the fact that the number of these systems connected to the grid is always increasing. This means that it is very important to control the harmonics generated by these inverters to limit their adverse effects on the grid power quality. IEEE and European IEC standards (IEEE 929, IEEE 1547 and IEC 61727) suggest harmonic limits generated by Photovoltaic (PV) Systems and Distributed Power Resources for the current total harmonic distortion (THD) factor and also for the magnitude of each harmonic.

The current controller can have a significant effect on the quality of the current supplied to the grid by the PV inverter, and therefore it is important that the controller provides a high quality sinusoidal output with minimal distortion to avoid creating harmonics. A commonly used current controller for Grid-Connected PV Inverters is the PR current controller. This controller is highly suited to operate with sinusoidal references like the reference used in Grid-Connected PV

* Corresponding author.
E-mail address: daniel.zammit@um.edu.mt (D. Zammit).
Peer review under the responsibility of Electronics Research Institute (ERI).

Production and hosting by Elsevier

http://dx.doi.org/10.1016/j.jesit.2017.01.003

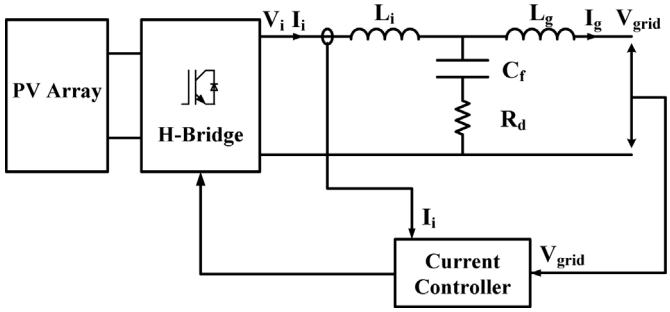

Fig. 1. Block diagram of the Grid-Connected PV Inverter with the LCL Filter.

Inverters, thus making it an optimal solution for this application. The PR controller provides gain at a certain frequency (resonant frequency) and almost no gain exists at the other frequencies.

The PR current controller is presented and discussed in Teodorescu et al. (2004), Liserre et al. (2005a), and Ciobotaru et al. (2005). Although this controller has a high ability to track a sinusoidal reference such as a current waveform, the output current of the grid-connected inverter is not immune from harmonic content (Zammit et al., 2014). Harmonics in the output current can result due to the converter non-linearities as well as from harmonics which are already present in the grid. Selective harmonics in the current can be compensated by using additional PR controllers which act at particular harmonic frequencies to be reduced or eliminated such as the 3rd, 5th, 7th and so on. This compensation can be used to reduce the current THD and make the inverter compliant to the IEEE and IEC standards (Teodorescu et al., 2004; Teodorescu et al., 2006; Castilla et al., 2009).

This paper presents the design procedure of a PR current controller and selective harmonic compensation applied for the 3rd, 5th and 7th harmonics. The design of the current control and harmonic compensation was carried out using Matlab's SISO Design Tool and the Bode diagram of the system. Results from testing of the PR current control on its own and with additional harmonic compensators as used in Grid-Connected PV Inverters is presented, both by simulations and by experimental tests. Experimental testing was carried out on a single phase 3 kW Grid-Connected PV Inverter, which was designed and built for this research.

Fig. 1 below shows the block diagram of the Grid-Connected PV Inverter system connected to the grid through an LCL filter used for this research.

This paper is divided into six sections. Section 2 covers the theory for the LCL filter and the current control, while Section 3 covers the design of the LCL filter, the PR current control and the harmonic compensators. Sections 4 and 5 present the simulations and inverter testing, respectively. These are followed by Section 6 which covers the comparison of results of the PR current control alone with the PR current control including the additional harmonic compensators. This paper concludes with final comments in Section 7.

2. LCL filter and current control

2.1. LCL filter

The transfer function of the LCL filter of Fig. 1 in terms of the inverter current I_i and the inverter voltage U_i, neglecting R_d, is:

$$G_F(s) = \frac{I_i}{U_i} = \frac{1}{L_i s} \frac{\left(s^2 + \left(\frac{1}{L_g C_f}\right)\right)}{\left(s^2 + \left(\frac{L_i + L_g}{L_i L_g C_f}\right)\right)} \tag{1}$$

where, L_i is the inverter side inductor, L_g is the grid side inductor, and C_f is the filter capacitor.

The resonant frequency of the filter is given by:

$$\omega_{res} = \sqrt{\frac{(L_i + L_g)}{(L_i L_g C_f)}} \tag{2}$$

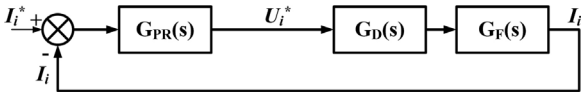

Fig. 2. The PR current control.

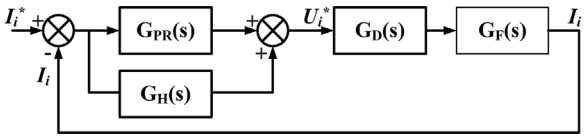

Fig. 3. The PR current control with harmonic compensators.

The transfer function in (1) does not include the damping resistor R_d. The introduction of R_d in series with the capacitor C_f increases stability and reduces resonance (Pradeep et al., 2004). This method of damping is a type of passive damping. Whilst there exist other methods of passive damping and also more advanced active damping methods, this particular damping method used was considered enough for the aim and purpose of this research due to its simplicity. The transfer function of the filter taking in consideration the damping resistor R_d is:

$$G_F(s) = \frac{I_i}{U_i} = \frac{1}{L_i s} \frac{\left(s^2 + s\left(\frac{R_d}{L_g}\right) + \left(\frac{1}{L_g C_f}\right)\right)}{\left(s^2 + s\left(\frac{(L_i+L_g)R_d}{L_i L_g}\right) + \left(\frac{L_i+L_g}{L_i L_g C_f}\right)\right)} \tag{3}$$

2.2. PR control

Fig. 2 below shows the PR current control strategy. I_i is the inverter output current, I_i^* is the inverter current reference and U_i^* is the inverter voltage reference.

The PR current controller $G_{PR}(s)$ is represented by:

$$G_{PR}(s) = K_P + K_I \frac{s}{s^2 + {\omega_0}^2} \tag{4}$$

where, K_P is the Proportional Gain term, K_I is the Integral Gain term and ω_0 is the resonant frequency.

$G_F(s)$ represents the LCL filter. $G_D(s)$ represents the processing delay of the microcontroller, which is typically equal to the time of one sample T_s and is represented by:

$$G_D(s) = \frac{1}{1 + sT_s} \tag{5}$$

The ideal resonant term on its own in the PR controller provides an infinite gain at the ac frequency ω_0 and no phase shift and gain at the other frequencies (Teodorescu et al., 2011). The K_P term determines the dynamics of the system; bandwidth, phase and gain margins (Teodorescu et al., 2011).

Eq. (4) represents an ideal PR controller which can give stability problems because of the infinite gain. To avoid these problems, the PR controller can be made non-ideal by introducing damping as shown in (6) below.

$$G_{PR}(s) = K_P + K_I \frac{2\omega_c s}{s^2 + 2\omega_c s + {\omega_0}^2} \tag{6}$$

where, ω_c is the bandwidth around the ac frequency of ω_0.

With (6) the gain of the PR controller at the ac frequency ω_0 is now finite but it is still large enough to provide only a very small steady state error. This equation also makes the controller more easily realizable in digital systems due to their finite precision (Zmood and Holmes, 2003).

2.3. PR control with harmonic compensators

Fig. 3 below shows the PR current control with an additional harmonic compensation block $G_H(s)$.

The harmonic compensator $G_H(s)$ is represented by:

$$G_H(s) = \sum_{h=3,5,7,\ldots} K_{Ih} \frac{s}{s^2 + (h\omega_0)^2} \tag{7}$$

where, K_{Ih} is the Resonant term at the particular harmonic and $h\omega_0$ is the resonant frequency of the particular harmonic.

The harmonic compensator for each harmonic frequency is added to the fundamental frequency PR controller to form the complete current controller, as shown in Fig. 3.

Eq. (7) represents an ideal harmonic compensator which as stated for the fundamental PR controller, can give stability problems due to the infinite gain. To avoid these problems, the harmonic compensator equation can be made non-ideal by representing it using (8).

$$G_H(s) = \sum_{h=3,5,7,\ldots} K_{Ih} \frac{2\omega_c s}{s^2 + 2\omega_c s + (h\omega_0)^2} \tag{8}$$

where, ω_c is the bandwidth around the particular harmonic frequency of $h\omega_0$.

As for the case of the fundamental PR controller, with (8) the gain of the harmonic compensator at the harmonic frequency $h\omega_0$ is now finite but it is still large enough to provide compensation.

3. LCL filter, PR controller and harmonic compensators design

3.1. Inverter and LCL filter design parameters

To carry out the tests using the PR control and the harmonic compensation, a 3 kW Grid-Connected Inverter was designed and constructed. The LCL filter was designed following the procedure in Teodorescu et al. (2011) and Liserre et al. (2005b). Designing for a dc-link voltage of 358 V, maximum ripple current of 20% of the grid peak current, a switching frequency of 10 kHz, filter cut-off frequency of 2 kHz and the capacitive reactive power not exceeding 5% of rated power, the following values of the LCL filter were obtained: $L_i = 1.2$mH, $L_g = 0.7$mH, $C_f = 9\ \mu$F and $R_d = 8\ \Omega$.

3.2. PR controller design

The block diagram of the complete system used to design the control is shown in Fig. 2. In the inverter current feedback path an Anti-aliasing filter was used to prevent the aliasing effect when sampling the inverter current. The Anti-Aliasing filter used was a second order non-inverting active low pass filter using the Sallen-Key filter implementation and a Butterworth design with cut-off frequency of 2.5 kHz.

The optimal fundamental PR current controller design was carried out using SISO Tool in Matlab. To design the optimal controller, the integral gain K_I at the ac frequency ω_0 must be set large enough to enforce only a very small steady state error, and also set the proportional gain K_P value to obtain sufficient bandwidth accommodating the other harmonic compensators which would otherwise cause system instability. The PR controller was designed for a resonant frequency ω_0 of 314.16 rad/s (50 Hz) and ω_c was set to be 0.5 rad/s, obtaining a K_P of 6.8 and K_I of 1498.72, shown in (9).

$$G_{PR}(s) = 6.8 + 1498.72 \frac{s}{s^2 + s + (2\pi\,(50))^2} \tag{9}$$

Fig. 4 shows the root locus plot in Matlab of the system including the LCL filter, the processing delay, anti-aliasing filter in the output current feedback path and the PR controller. The root locus plot shows that the designed system is stable.

Figs. 5 and 6 show the open loop bode diagram and the closed loop bode diagram of the system, respectively. From the open loop bode diagram, the Gain Margin obtained is 13.9 dB at a frequency of 9970 rad/s and the Phase Margin obtained is 51° at a frequency of 3300 rad/s.

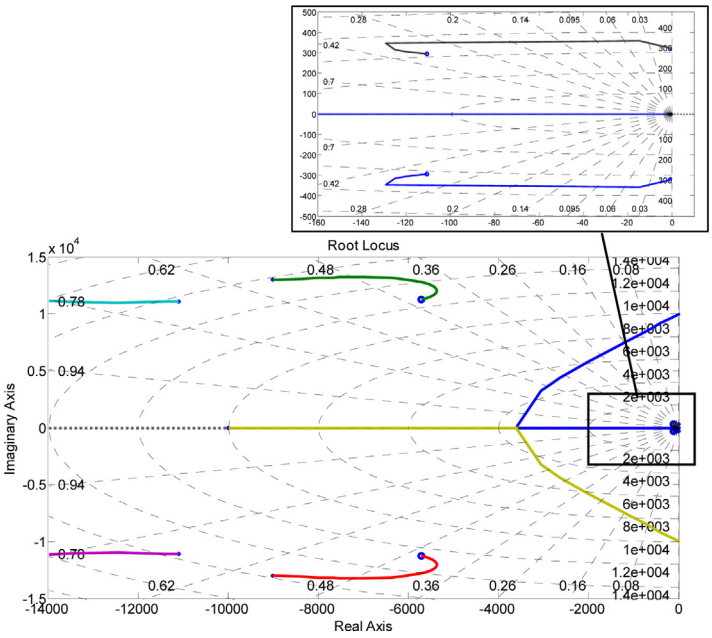

Fig. 4. Root locus of the inverter with the PR controller.

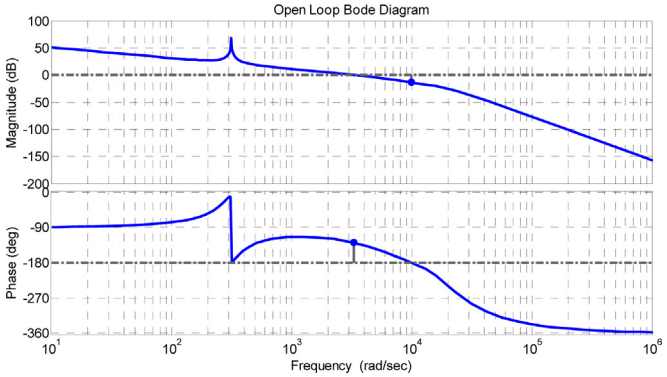

Fig. 5. Open loop bode diagram of the system with PR control.

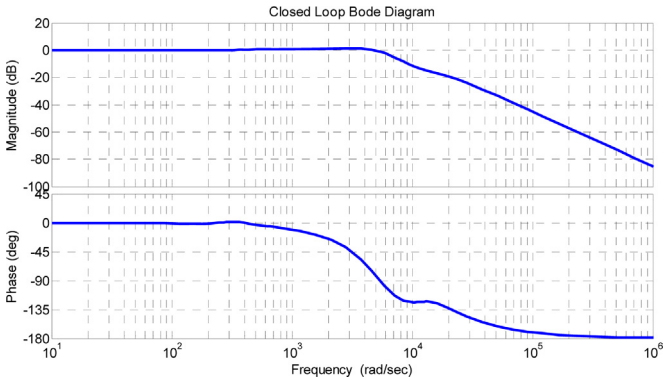

Fig. 6. Closed loop bode diagram of the system with PR control.

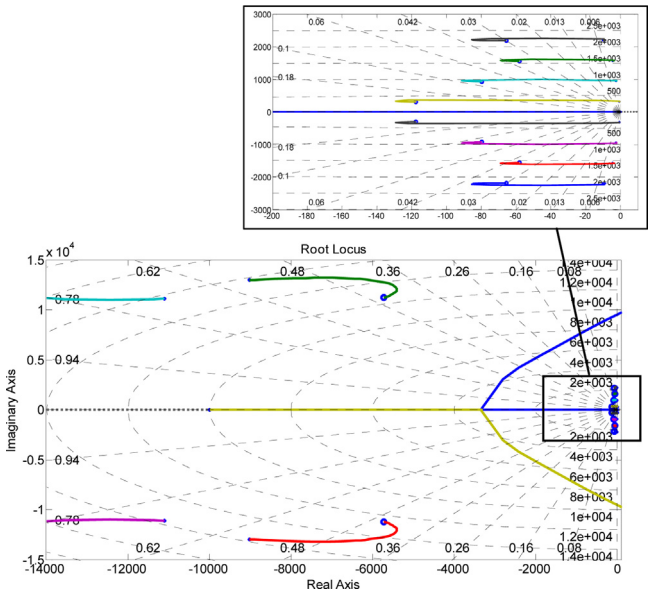

Fig. 7. Root locus of the inverter with the fundamental PR controller and the harmonic compensators.

3.3. Harmonic compensators design

The block diagram of the complete system used to design the selective harmonic compensators is shown in Fig. 3. In the inverter current feedback path an Anti-aliasing filter was used to prevent the aliasing effect when sampling the inverter current.

Harmonic compensators were designed for the 3rd, 5th and 7th harmonics. The PR harmonic compensators were designed using SISO Tool in Matlab with the resonant frequency set to the particular frequency to be compensated, i.e. 150 Hz for the 3rd harmonic, 250 Hz for the 5th harmonic and 350 Hz for the 7th harmonic. Similarly to the fundamental PR current control design, the Root Locus, Open Loop and Closed Loop Bode diagrams plotted by SISO Tool were used to achieve the optimal design for each harmonic compensator. Each harmonic compensator was designed on its own and then combined together with the fundamental PR controller at the end in SISO Tool. Ultimately fine tuning of the compensators was performed to obtain the optimum operation of the compensators by varying ω_c and K_I of the corresponding compensator. Care was taken that the system remains stable, by using the gain margin and phase margin stability criteria.

The 3rd harmonic compensator at a resonant frequency $3\omega_0$ of 942.48 rad/s (150 Hz) was designed with a ω_c of 2.5 rad/s and a K_I of 211.208. The 5th harmonic compensator at a resonant frequency $5\omega_0$ of 1570.8 rad/s (250 Hz) was designed with a ω_c of 4.5 rad/s and a K_I of 83.867. The 7th harmonic compensator at a resonant frequency $7\omega_0$ of 2199.11 rad/s (350 Hz) was designed with a ω_c of 10 rad/s and a K_I of 40.834. The transfer function of the complete controller $G_C(s)$ is shown in (10).

$$G_C(s) = G_{PR}(s) + G_{3H}(s) + G_{5H}(s) + G_{7H}(s) = \frac{6.8\left(s^2 + 221.4s + (2\pi \times 50)^2\right)}{s^2 + s + (2\pi \times 50)^2} + \frac{1056.04s}{s^2 + 5s + (2\pi \times 150)^2} + \frac{754.8s}{s^2 + 9s + (2\pi \times 250)^2} + \frac{816.68s}{s^2 + 20s + (2\pi \times 350)^2} \tag{10}$$

Fig. 7 shows the root locus plot in Matlab of the system with the additional harmonic compensators. The root locus plot shows that the designed system is stable.

Figs. 8 and 9 show the open loop bode diagram and the closed loop bode diagram of the system, respectively. From the open loop bode diagram, the Gain Margin obtained is 13.2 dB at a frequency of 9520 rad/s and the Phase Margin obtained is 41.8° at a frequency of 3310 rad/s.

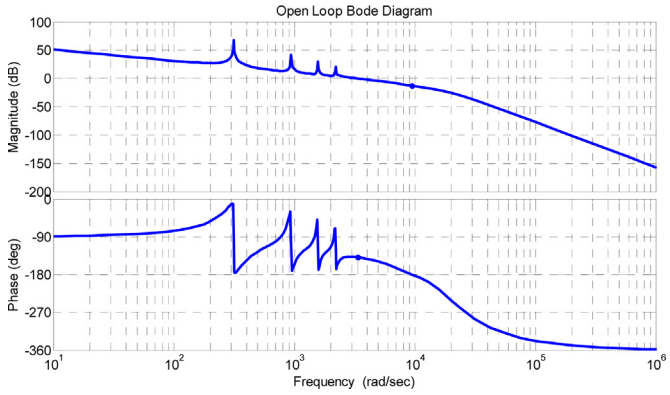

Fig. 8. Open loop bode diagram of the system with the fundamental PR controller and the harmonic compensators.

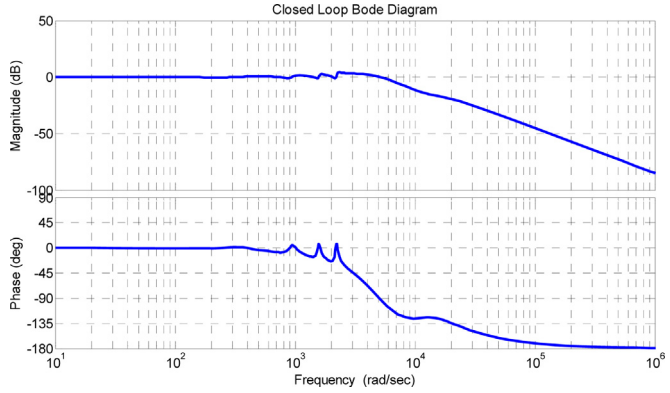

Fig. 9. Closed loop bode diagram of the system with the fundamental PR controller and the harmonic compensators.

4. Simulations

The 3 kW Grid-Connected PV Inverter was modeled and simulated in Simulink with PLECS blocksets. The grid voltage was set to 325 V peak (230 V rms), the dc-link voltage was set to 360 V and the reference current was set to 18.446A peak to simulate a 3 kW inverter. 3rd, 5th and 7th harmonics were added to the grid voltage corresponding to a Total Harmonic Distortion (THD) of 3.37%, to distort the grid voltage sinusoidal waveform. Simulations were carried out to observe the effect of the harmonics with and without harmonic compensation on the inverter voltage and grid current.

Figs. 10 and 11 show the inverter voltage (V_{pwm}), the grid voltage (V_{grid}), the capacitor voltage (V_{cap}), the inverter current (I_{inv}), the grid current (I_{grid}) and the reference current (I_{ref}) from the simulation using the PR controller without and with harmonic compensation, respectively. Figs. 12 and 13 show the harmonic spectrum of the grid current from the simulation using the PR controller without and with harmonic compensation, respectively.

From the simulation results without harmonic compensation shown in Figs. 10 and 12 it can be seen that the grid current I_{grid} was highly affected by the harmonics present in the grid voltage. When considering the harmonics of the grid current as a percentage of the reference current, the 3rd, 5th and 7th harmonics were about 8.528%, 3.44% and 1.649%, respectively. When the harmonic compensators were applied, the 3rd, 5th and 7th harmonics in the grid current I_{grid} were reduced to 0.613%, 0.474% and 0.388%, respectively, as can be seen from the simulation results shown in Figs. 11 and 13.

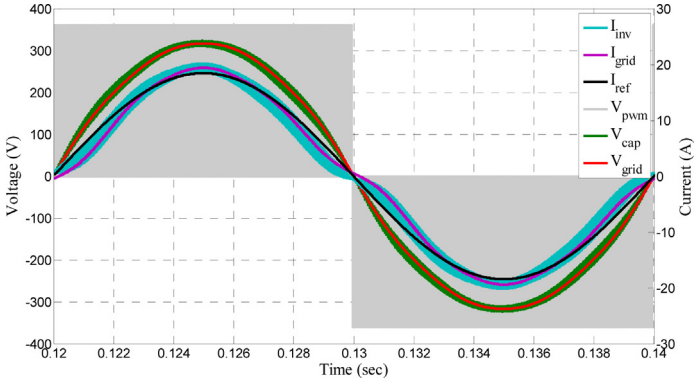

Fig. 10. Simulation result from the inverter with PR current control without harmonic compensation.

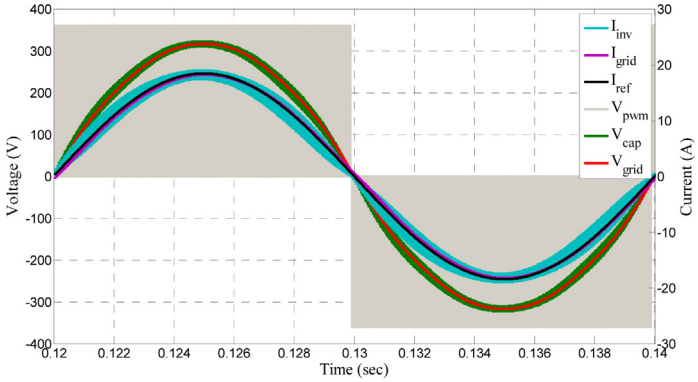

Fig. 11. Simulation result from the inverter with PR current control with harmonic compensation.

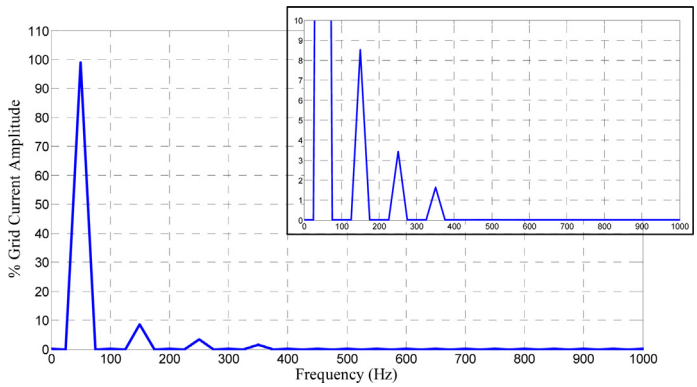

Fig. 12. Simulation grid current harmonic spectrum with PR Current control without harmonic compensation.

5. Grid-Connected PV Inverter testing

The constructed 3 kW Grid-Connected PV Inverter test rig is shown in Fig. 14. The inverter was operated at a switching frequency of 10 kHz and was connected to a 50 Hz grid supply. The inverter was controlled by the Microchip dsPIC30F4011 microcontroller. Testing was carried out using the PR controller without and with the selective harmonic compensators to analyze the performance of the compensators. The inverter was connected to the grid using a variac to allow variation of the grid voltage for testing purposes. The dc link voltage was obtained from a dc power supply.

Tests were performed to measure the harmonics present in the grid voltage. The 3rd, 5th and 7th harmonics present in the grid voltage were typically about 0.9%, 1.912% and 0.231%, respectively. Fig. 15 shows the inverter output

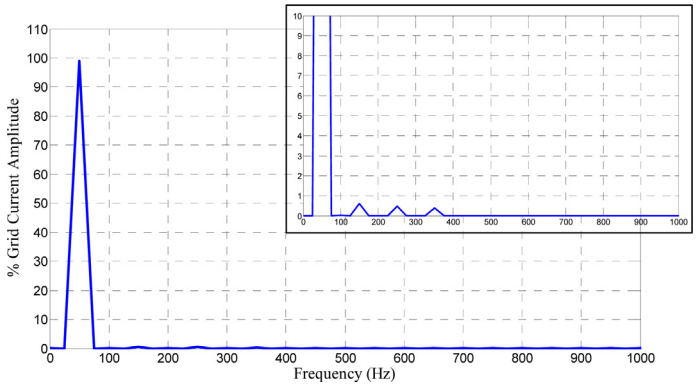

Fig. 13. Simulation grid current harmonic spectrum with PR current control with harmonic compensation.

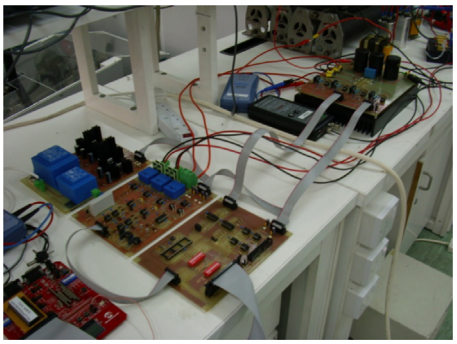

Fig. 14. 3 kW Grid-Connected PV Inverter test rig.

voltage, the grid voltage and the grid current for a dc-link voltage of 300 V, a grid voltage of 154 V and a preset reference value of 8A peak using the PR current controller (a) without harmonic compensation, (b) with 3rd harmonic compensation, (c) with 3rd and 5th harmonic compensation and (d) with 3rd, 5th and 7th harmonic compensation, respectively. Fig. 16 shows the grid current for the grid-connected inverter with the PR current controller (a) without harmonic compensation, (b) with 3rd harmonic compensation, (c) with 3rd and 5th harmonic compensation and (d) with 3rd, 5th and 7th harmonic compensation, respectively. I_g is the grid current, I_{gr} is the reconstructed grid current up to its 13th harmonic (a reconstruction of the grid current by adding the first 13 lower harmonics) and I_{gfund} is the fundamental component of the grid current.

Fig. 17 shows the harmonic spectrum of the grid current with PR current control (a) without harmonic compensation, (b) with 3rd harmonic compensation, (c) with 3rd and 5th harmonic compensation and (d) with 3rd, 5th and 7th harmonic compensation, respectively. Without harmonic compensation the 3rd, 5th and 7th harmonics resulted about 5.574%, 4.231% and 2.435% of the reference value of 8A peak, respectively. When the harmonic compensators were used the 3rd, 5th and 7th harmonics resulted about 0.378%, 0.641% and 0.24% of the reference value of 8A peak, respectively.

6. Comparison of experimental results

The 3rd, 5th and 7th harmonics in the grid voltage were typically about 0.9%, 1.912% and 0.231%, respectively. Table 1 shows the percentage fundamental and harmonic content of the grid current for the PR current controlled grid-connected inverter without and with the selective harmonic compensators. The percentage calculations for the grid current are based on the reference current of 8A peak. As can be observed from the experimental results, the harmonic compensators have drastically reduced the 3rd, 5th and 7th harmonics in the grid current. This agrees with the results obtained in the simulations. These harmonics could be reduced further by increasing the gain of the compensators at the harmonic frequency, but this could possibly cause system instability. This could happen because by increasing the gain, the phase peaks/dips at the harmonic frequencies would also increase, cutting the -180° line and thus providing

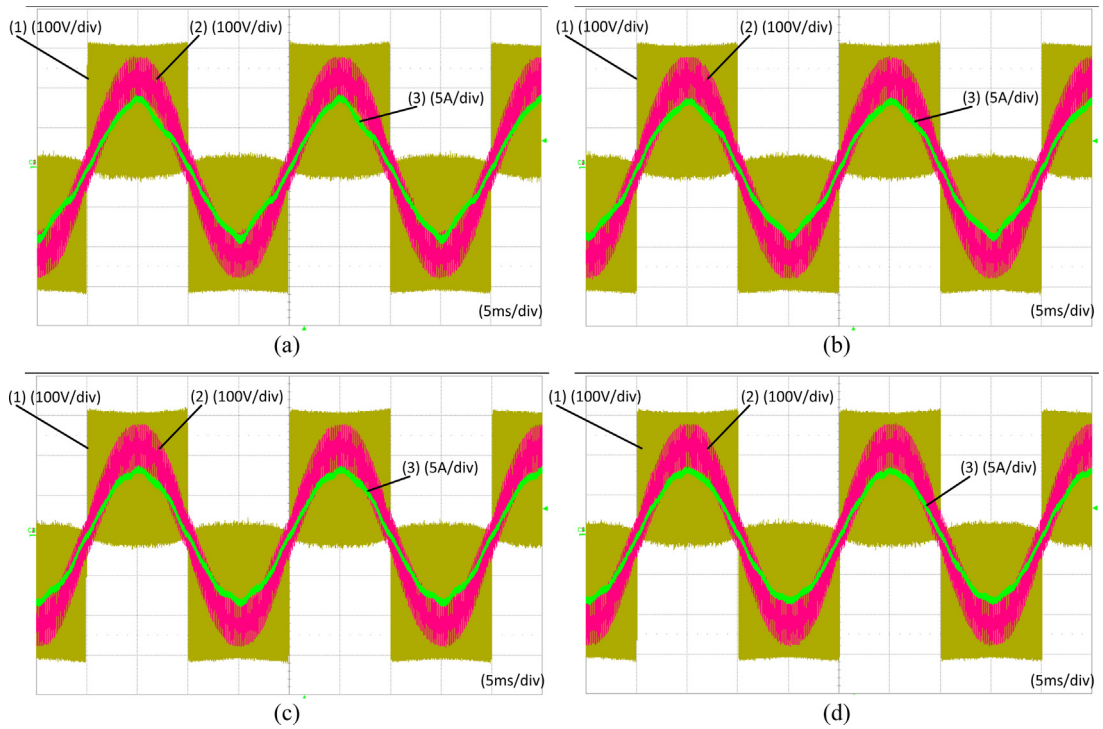

Fig. 15. Inverter output voltage (1), grid voltage (2) and grid current (3) with a preset current of 8A peak using (a) the PR controller without harmonic compensation, (b) the PR controller with 3rd harmonic compensation, (c) the PR controller with 3rd and 5th harmonic compensation, (d) the PR controller with 3rd, 5th and 7th harmonic compensation.

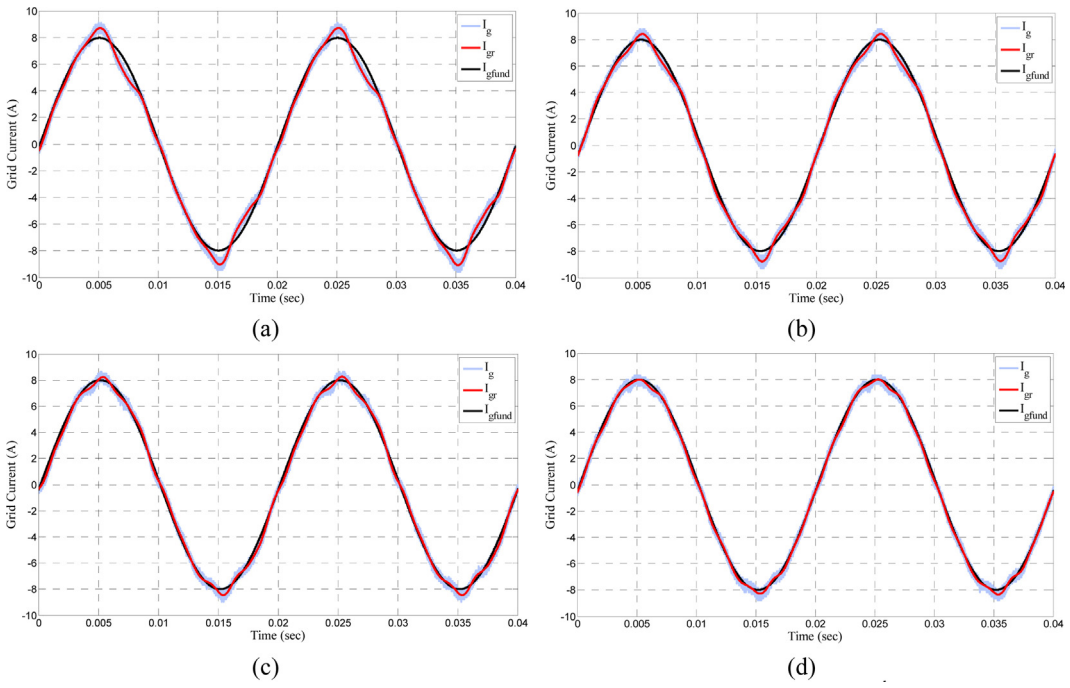

Fig. 16. Grid current with PR current control (a) without harmonic compensation, (b) with 3rd harmonic compensator, (c) with 3rd and 5th harmonic compensators, (d) with 3rd, 5th and 7th harmonic compensators.

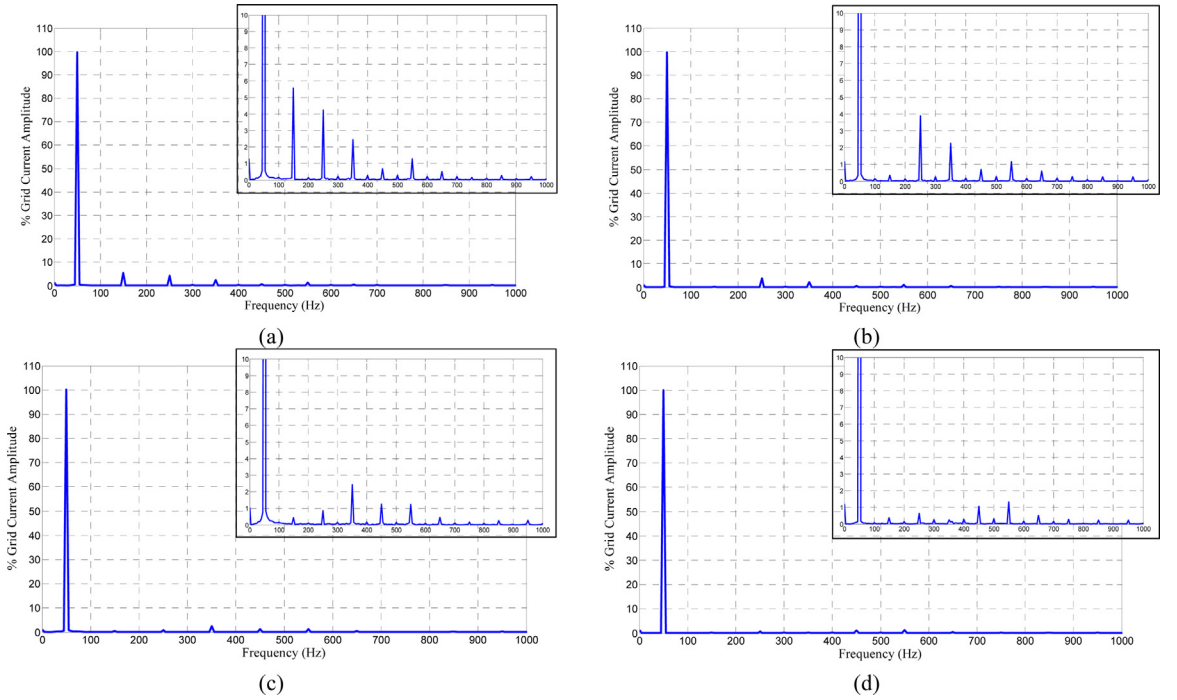

Fig. 17. Harmonic spectrum of the grid current with PR current control (a) without harmonic compensation, (b) with the 3rd harmonic compensator, (c) with the 3rd and 5th harmonic compensators, (d) with the 3rd, 5th and 7th harmonic compensators.

Table 1
Fundamental and harmonics for the PR current controlled grid-connected inverter with selective harmonic compensation.

	Fund	3th harm	5th harm	7th harm
	I_g	I_g	I_g	I_g
Fundamental PR only	100%	5.574%	4.231%	2.435%
Fund PR, 3rd H. comp	100%	0.352%	3.893%	2.257%
Fund PR, 3rd, 5th H. comp	100%	0.448%	0.862%	2.437%
Fund PR, 3rd, 5th, 7th H. comp	100%	0.378%	0.641%	0.24%

a negative gain margin that drives the system unstable. As can be observed from the open loop bode diagram in Fig. 10 the phase dips are already at the maximum possible. A possible solution might be to increase the bandwidth of the system by increasing the proportional gain K_P of the fundamental PR controller, making room for larger gains for the harmonic compensators. However by increasing the bandwidth of the system the chance of being affected by higher harmonics (9th, 11th, 13th and so on) is increased, leading to the need of additional harmonic compensators on those harmonics too. Therefore a compromise has to be found, obtain the lowest harmonics possible with also the narrowest bandwidth possible.

The IEEE 929 and IEEE 1547 standards allow a limit of 4% for each harmonic from 3rd to 9th and 2% for 11th to 15th (IEEE, 2000; IEEE, 2003). The IEC 61727 standard specifies similar limits (IEC, 2004). As can be observed from the results obtained the 3rd and 5th harmonics were above the limit when no harmonic compensation was applied. These harmonics result from the inverter non-linearities and also from the harmonics already present in the grid supply. The harmonic compensators reduced the 3rd and 5th harmonics within the limits and reduced further the 7th harmonic, thus making the inverter compliant to the standard regulations.

7. Conclusion

This paper presented a procedure to design a Proportional Resonant (PR) current control with additional selective harmonic compensators for Grid Connected Photovoltaic (PV) Inverters. A 3 kW grid connected PV inverter was designed and built for this research. This paper covered the design of the PR control and also the design of the selective harmonic compensators for the 3rd, 5th and 7th harmonics. Results from simulations and experimental analysis of the inverter with PR current control and harmonic compensation were presented. Both simulation and experimental results showed the effectiveness of the harmonic compensators to reduce the harmonics in the grid current. The 3rd, 5th and 7th harmonics in the grid current were reduced from about 5.574%, 4.231% and 2.435%, respectively, to about 0.378%, 0.641% and 0.24%, respectively. This reduction in harmonics made the grid connected inverter compliant to the standard regulations.

References

Castilla, M., Miret, J., Matas, J., de Vicuna, L.G., Guerrero, J.M., 2009. Control design guidelines for single-phase grid-connected photovoltaic inverters with damped resonant harmonic compensators. IEEE Trans. Ind. Power Electron. 56 (11).

Ciobotaru, M., Teodorescu, R., Blaabjerg, F., 2005. Control of a Single-Phase PV Inverter. EPE2005, Dresden.

IEC 61727 2004 Standard Photovoltaic (PV) Systems-Characteristics of the Utility Interface.

IEEE 929 2000 Recommended Practice for Utility Interface of Photovoltaic (PV) Systems.

IEEE 1547 2003 Standard for Interconnecting Distributed Resources with Electric Power Systems.

Liserre, M., Teodorescu, R., Chen, Z., 2005a. Grid Converters and Their Control in Distributed Power Generation Systems. IECON 2005 Tutorial.

Liserre, M., Blaabjerg, F., Hansen, S., 2005. Design and control of an LCL-filter based three phase active rectifier. IEEE Trans. Ind. Appl. 41 (September/October (5)).

Pradeep, V., Kolwalkar, A., Teichmann, R., 2004. Optimized Filter Design for IEEE 519 Compliant Grid Connected Inverters. IICPE 2004, Mumbai, India.

Teodorescu, R., Blaabjerg, F., Borup, U., Liserre, M., 2004. A new control structure for grid-connected LCL PV inverters with zero steady-state error and selective harmonic compensation. In: APEC'04 Nineteenth Annual IEEE Conference, California.

Teodorescu, R., Blaabjerg, F., Liserre, M., Loh, P.C., 2006. Proportional-resonant controllers and filters for grid-connected voltage-source converters. IEEE Proc. Electr. Power Appl. 153 (5).

Teodorescu, R., Liserre, M., Rodriguez, P., 2011. Grid Converters for Photovoltaic and Wind Power Systems. Wiley.

Zammit, D., Spiteri Staines, C., Apap, M., 2014. Comparison between PI and PR current controllers in grid connected PV inverters, WASET. Int. J. Electr. Electron. Sci. Eng. 8 (2).

Zmood, D.N., Holmes, D.G., 2003. Stationary frame current regulation of PWM inverters with zero steady-state error. IEEE Trans. Power Electron. 18 (3).